

## Article

# Synthesis, Crystal Structure and Properties of the New Laminar Quaternary Tellurides $\text{SrLnCuTe}_3$ ( $\text{Ln} = \text{Sm}, \text{Gd-Tm}$ and $\text{Lu}$ )

Anna V. Ruseikina <sup>1,\*</sup>, Maxim V. Grigoriev <sup>1,2</sup>, Maxim S. Molokeev <sup>3,4,5</sup>, Alexander A. Garmonov <sup>6</sup>, Andrey V. Elyshev <sup>1</sup>, Ralf J. C. Locke <sup>2</sup> and Thomas Schleid <sup>2,\*</sup>

<sup>1</sup> Laboratory of Theory and Optimization of Chemical and Technological Processes, University of Tyumen, 625003 Tyumen, Russia

<sup>2</sup> Institute for Inorganic Chemistry, University of Stuttgart, D-70569 Stuttgart, Germany

<sup>3</sup> Kirensky Institute of Physics, Federal Research Center KSC SB RAS, 660036 Krasnoyarsk, Russia

<sup>4</sup> Department of Engineering Physics and Radioelectronic, Siberian Federal University, 660041 Krasnoyarsk, Russia

<sup>5</sup> Department of Physics, Far Eastern State Transport University, 680021 Khabarovsk, Russia

<sup>6</sup> Institute of Physics and Technology, University of Tyumen, 625003 Tyumen, Russia

\* Correspondence: a.v.ruseikina@utmn.ru (A.V.R.); thomas.schleid@iac.uni-stuttgart.de (T.S.)

**Abstract:** This paper reports for the first time on the new laminar quaternary orthorhombic heterometallic quaternary tellurides  $\text{SrLnCuTe}_3$ , the fabrication of which has been a challenge until this work. Data on the crystal structure of tellurides complete the series of quaternary strontium chalcogenides  $\text{SrLnCuCh}_3$  ( $\text{Ch} = \text{S}, \text{Se}, \text{Te}$ ). Single crystals of the compounds were synthesized from the elements by the halogenide-flux method at 1070 K. The compounds are crystallizing in two space groups  $Pnma$  ( $\text{Ln} = \text{Sm}, \text{Gd}$  and  $\text{Tb}$ ) and  $Cmcm$  ( $\text{Ln} = \text{Dy-Tm}$  and  $\text{Lu}$ ). For  $\text{SrSmCuTe}_3$  ( $a = 11.4592(7)$ ,  $b = 4.3706(3)$ ,  $c = 14.4425(9)$  Å, space group:  $Pnma$ ) with the largest lanthanoid cation,  $\text{Sr}^{2+}$  shows  $C.N. = 7$ , whereas  $\text{Sm}^{3+}$  reveals a diminished coordination number  $C.N. = 6$ . For  $\text{SrLuCuTe}_3$  ( $a = 4.3064(3)$ ,  $b = 14.3879(9)$ ,  $c = 11.1408(7)$  Å, space group:  $Cmcm$ ) with the smallest lanthanoid cation, coordination numbers of six are realized for both high-charged cations ( $\text{Sr}^{2+}$  and  $\text{Lu}^{3+}$ ;  $C.N. = 6$ ). The cations  $\text{Sr}^{2+}$ ,  $\text{Ln}^{3+}$ ,  $\text{Cu}^{+}$  each take independent positions. The structures are built by distorted  $[\text{CuTe}_4]^{7-}$  tetrahedra, forming the infinite chains  $\infty 1\{[\text{Cu}(\text{Te}1)1/1t(\text{Te}2)1/1t(\text{Te}3)2/2e]^{5-}\}$  along  $[010]$  in  $\text{SrLnCuTe}_3$  ( $\text{Ln} = \text{Sm}, \text{Gd}$  and  $\text{Tb}$ ) and  $[100]$  in  $\text{SrLnCuTe}_3$  ( $\text{Ln} = \text{Dy-Tm}$  and  $\text{Lu}$ ). The distortion of the polyhedra  $[\text{CuTe}_4]^{7-}$  was compared for the whole series  $\text{SrLnCuTe}_3$  by means of  $\tau_4$ -descriptor for the four coordinating  $\text{Te}^{2-}$  anions, which revealed a decrease in the degree of distortion with a decreasing radius at  $\text{Ln}^{3+}$ . The distorted octahedra  $[\text{LnTe}_6]^{9-}$  form layers  $\infty 2\{[\text{Ln}(\text{Te}1)2/2(\text{Te}2)2/2(\text{Te}3)2/2]^{3-}\}$ . The distorted octahedra and tetrahedra fuse to form parallel layers  $\infty 2\{[\text{CuLnTe}_3]^{2-}\}$  and between them, the  $\text{Sr}^{2+}$  cations providing three-dimensionality of the structure are located. In the  $\text{SrLnCuTe}_3$  ( $\text{Ln} = \text{Sm}, \text{Gd}$  and  $\text{Tb}$ ) structures, the  $\text{Sr}^{2+}$  cations center capped the trigonal prisms  $[\text{SrTe}_{6+1}]^{12-}$ , united in infinite chains  $\infty 1\{[\text{Sr}(\text{Te}1)2/2(\text{Te}2)3/3(\text{Te}3)2/2]^{4-}\}$  along the  $[100]$  direction. The domains of existence of the  $\text{Ba}_2\text{MnS}_3$ ,  $\text{BaLaCuS}_3$ ,  $\text{Eu}_2\text{CuS}_3$  and  $\text{KZrCuS}_3$  structure types are defined in the series of orthorhombic chalcogenides  $\text{SrLnCuCh}_3$  ( $\text{Ch} = \text{S}, \text{Se}$  and  $\text{Te}$ ). The tellurides  $\text{SrLnCuTe}_3$  ( $\text{Ln} = \text{Tb-Er}$ ) of both structure types in the temperature range from 2 up to 300 K are paramagnetic, without showing clear signs of a magnetic phase transition.

**Keywords:** quaternary tellurides; lanthanoids; synthesis; crystal structures; magnetic properties



**Citation:** Ruseikina, A.V.; Grigoriev, M.V.; Molokeev, M.S.; Garmonov, A.A.; Elyshev, A.V.; Locke, R.J.C.; Schleid, T. Synthesis, Crystal Structure and Properties of the New Laminar Quaternary Tellurides  $\text{SrLnCuTe}_3$  ( $\text{Ln} = \text{Sm}, \text{Gd-Tm}$  and  $\text{Lu}$ ). *Crystals* **2023**, *13*, 291. <https://doi.org/10.3390/cryst13020291>

Academic Editor: Andrei Vladimirovich Shevelkov

Received: 31 December 2022

Revised: 1 February 2023

Accepted: 6 February 2023

Published: 9 February 2023



**Copyright:** © 2023 by the authors. Licensee MDPI, Basel, Switzerland. This article is an open access article distributed under the terms and conditions of the Creative Commons Attribution (CC BY) license (<https://creativecommons.org/licenses/by/4.0/>).

## 1. Introduction

Recently, the study of four-component tellurides with various combinations of  $s$ -,  $d$ - and  $f$ -elements [1–13] has been of great scientific interest that is associated with their interesting structural features and potential valuable properties. The formation of various telluride coordination polyhedra centered by cations and their various combinations with

each other in quaternary tellurides result in the formation of a wide range of layer or channel structures and provide the potential of changing the band gap, as well as electrical and optical characteristics [14–21]. Tellurides exerting various properties like diamagnetic [19], paramagnetic [22,23] or antiferromagnetic [10,19] are *p*-type semiconductors [10,22,23] or exhibit metallic properties [5,23]. Based on ab initio calculation methods, a low thermal lattice conductivity of thermodynamically stable-layered quaternary tellurides  $AEREMTe_3$  ( $AE$  = alkaline-earth element;  $RE$  = rare-earth element;  $M$  = *d*-element) has been recently predicted, which allows them to be used as thermoelectric materials [1,21]. The effect of lone pairs on the structural features of  $BaRECuTe_3$  tellurides has been studied, and it was determined that the character of Ba–Te interactions are ionic, and  $RE$ –Te and Cu–Te interactions are of polar-covalent character [21]. Since the compounds of a number of quaternary barium tellurides  $BaRECuTe_3$  were synthesized as early as the end of the 20th century [3,18], it allowed them to remove the problem of the existence of all possible barium chalcogenides of the type  $BaRECuCh_3$  ( $Ch$  = S, Se and Te) [24,25]; then, in the case of strontium chalcogenides, the research works were focused only on the synthesis of the sulfide and selenide compounds [26–40] so far and only recently the first representative  $SrScCuTe_3$  of this telluride series was synthesized [2], the remaining representatives of the  $SrRECuTe_3$  series, as far as we know, have not been prepared. The existence of orthorhombic compounds of the entire  $SrRECuTe_3$  series, crystallizing in one space group ( $Pnma$ ) only, was predicted, notably the compounds  $SrRECuTe_3$  ( $RE$  = La–Nd, Sm, Gd–Lu and Y) belong to the  $Eu_2CuS_3$  structure type, and the compound  $SrScCuTe_3$  classes with the  $NaCuTiS_3$  structure type [1]. However, the scandium telluride  $SrScCuTe_3$ , experimentally prepared by the ampoule method after fusing stoichiometric amounts of the elements at 1273 K for 168 h, had the space group  $Cmcm$  [2]. The crystallization of scandium compounds in this space group is consistent with studies of layered quaternary chalcogenides  $AEScCuCh_3$  ( $AE$  = Sr [26,27,33], Eu [26,41], Ba [2];  $Ch$  = S [2,26,27], Se [2,27,33,41], Te [2]). The compounds with light rare-earth elements  $SrLnCuTe_3$  ( $Ln$  = La, Ce, Pr) are metastable according to theoretical calculations [1]. Over the past 20 years, several synthetic methods, such as the fusion of stoichiometric amounts of elements [2], the fusion of binary chalcogenides [28,30–32,34,38–40] and reductive chalcogenation of oxides [41], have been developed to prepare quaternary chalcogenides in the form of poly- and single-crystals line form; nevertheless, the halogenide-flux method turned out to be one of the most effective ones for both for a significant reduction in the time and temperature of synthesis and obtaining of homogeneous samples [4,10,18,20,22,23,33–37]. The experimental production of a series of quaternary strontium tellurides  $SrLnCuTe_3$  will make it possible to remove the question of the possibility of the existence of all possible quaternary strontium chalcogenides of the  $SrLnCuCh_3$  series ( $Ch$  = S, Se, Te) and will significantly complement fundamental research in the field of the chemistry of rare-earth chalcogenides.

The purpose of this research is to study a new series of quaternary tellurides with the formula  $SrLnCuTe_3$  ( $Ln$  = Sm, Gd–Tm and Lu), namely the development of synthesis, experimental determination of the crystal structures and magnetic properties.

## 2. Materials and Methods

### 2.1. Materials

The metals Sr (99.3%),  $Ln$  (La–Nd, Sm–Lu: 99.9%; Eu: 99.99%), Te (99.9%) and CsI (99.9%) were purchased from ChemPur (Karlsruhe, Germany). Cu (99.999%) was obtained from Aldrich (Milwaukee, WI, USA).

### 2.2. Synthesis

Single crystals of quaternary strontium tellurides  $SrLnCuTe_3$  ( $Ln$  = Sm, Gd–Tm and Lu) were synthesized by mixing in a glove box under argon atmosphere in a stoichiometric ratio of the elements strontium, copper, tellurium and a lanthanoid (1 Sr: 1 Cu: 1  $Ln$  ( $Ln$  = Sm, Gd–Tm and Lu): 3 Te) in the presence of an excess amount of the halogenide-flux CsI. The silica ampoules were evacuated to a pressure of  $2 \cdot 10^{-3}$  mbar and sealed. They were then heated

in a muffle furnace from room temperature to 1120 K for 30 h and kept at this temperature for 96 h, and after that cooled to 570 K at a rate of 4 K/h, then to room temperature within 3 h. The interaction proceeded according to the reaction:  $\text{Sr} + \text{Cu} + \text{Ln} + 3 \text{Te} \rightarrow \text{SrLnCuTe}_3$ . The heating profiles used for the synthesis of  $\text{SrLnCuTe}_3$  representatives with  $\text{Ln} = \text{Sm}, \text{Gd-Tm}$  and  $\text{Lu}$  are presented in Figure S1a in the Supplementary Materials. The reaction product was purified from flux residues with demineralized water. Black needle-shaped crystals of  $\text{SrLnCuTe}_3$  representatives were present in the product (Figure S1b,c in Supplementary Material). While the  $\text{SrLnCuTe}_3$  samples ( $\text{Ln} = \text{Tb-Er}$ ) after the removal of the flux were completely represented by single crystals of the  $\text{SrLnCuTe}_3$  compounds, in the  $\text{SrLnCuTe}_3$  ( $\text{Ln} = \text{Sm}, \text{Gd}, \text{Tm}$  and  $\text{Lu}$ ) samples the yield of single crystals was only 60–80%. The resulting crystals were suitable for single-crystal X-ray diffraction analysis. Unfortunately, it was not possible to obtain high-quality powder diffraction patterns (Figure S2).

We also tried to obtain quaternary chalcogenides  $\text{SrLnCuTe}_3$  ( $\text{Ln} = \text{La-Nd}, \text{Eu}$  and  $\text{Yb}$ ). Our repeated attempts were unsuccessful, however, during the synthesis, the interaction of the initial components was observed upon heating with the CsI flux, resulting in the formation of single crystals containing an alkali metal, namely  $\text{Cs}_x\text{Ln}_2\text{Cu}_{6-x}\text{Te}_6$  ( $\text{Ln} = \text{La-Nd}$ ) [19], and the samples also included single crystals of  $\text{Cu}_{0.37}\text{LnTe}_2$ ,  $\text{SrTe}$  and  $\text{LnTe}$  ( $\text{Ln} = \text{Eu}$  and  $\text{Yb}$ ). Disappointingly, single crystals of the  $\text{SrLnCuTe}_3$  phase were not found in the samples.

### 2.3. X-ray Diffraction Analysis

The intensities from single crystals of the  $\text{SrLnCuTe}_3$  series with  $\text{Ln} = \text{Sm}, \text{Gd-Tm}$  and  $\text{Lu}$  of  $0.05 \times 0.05 \times 0.45 \text{ mm}^3$  dimensions were collected at 293(2) K using SMART APEX II single-crystal diffractometer (Bruker AXS, Billerica, MA, USA) equipped with a CCD-detector, graphite monochromator and  $\text{Mo-K}_\alpha$  radiation source. The orientation matrix and cell parameters were determined and refined for a set of 11,880 reflections. The unit-cell parameters correspond to orthorhombic symmetry. The space groups ( $Pnma$  and  $Cmcm$ ) were determined from the statistical analysis of the intensities of all reflections. Absorption corrections were applied using the SADABS program. The structure was solved by the direct methods using packaged SHELXS and refined in the anisotropic approach using the SHELXL program [42]. The structural tests for the presence of missing symmetry elements and possible voids were produced using the PLATON program [43]. The crystallographic data are deposited in Cambridge Crystallographic Data Centre (CSD-2232062–2232066, 2232068–2232070). The data can be downloaded from the site [www.ccdc.cam.ac.uk/data\\_request/cif](http://www.ccdc.cam.ac.uk/data_request/cif) (accessed on 25 January 2023)

### 2.4. Powder X-ray Diffraction

The powder X-ray diffraction investigation was conducted using a STADI-P diffractometer (Stoe & Cie, Darmstadt, Germany) with Ge(111)-monochromatized molybdenum  $\text{K}_\alpha$ -radiation ( $\lambda = 71.07 \text{ pm}$ ) and copper  $\text{K}_\alpha$ -radiation ( $\lambda = 154.06 \text{ pm}$ ). Since copper compounds are strong absorbers of copper and strontium compounds for molybdenum radiation, we were not able to record high-quality powder X-ray diffractograms (PXRD, see Figure S2).

### 2.5. Electron-Beam Microprobe Analysis

The SEM image of  $\text{SrDyCuTe}_3$  was acquired using an electron-beam X-ray microprobe (SX-100, Cameca, Gennevilliers, France). The EDX spectra for several examples roughly confirmed the 1:1:1 stoichiometry of all investigated  $\text{SrLnCuTe}_3$  compounds.

### 2.6. Magnetic Measurements

The temperature dependencies of the magnetizations of the  $\text{SrLnCuTe}_3$  representatives with  $\text{Ln} = \text{Tb}, \text{Dy}, \text{Ho}$  and  $\text{Er}$  were measured by means of the magnetic-property measuring system with helium cooling (Quantum Design MPMS<sub>3</sub>, San Diego, CA, USA) in the temperature range from 2 to 300 K in zero-field cooling (ZFC) and heating in external magnetic field (FW) modes. The field strength was 500 kOe ( $0.4 \text{ MA} \cdot \text{m}^{-1}$ ). The dependencies of the

magnetizations on the magnitude of the external magnetic field were measured at room temperature (300 K) and at a temperature of 2 K, using a vibrating magnetometer as part of the same Quantum Design MPMS<sub>3</sub> system. The magnetic properties of the SrLnCuTe<sub>3</sub> compounds with Ln = Sm, Gd, Tm and Lu have not been studied because of the low yield of single crystals.

### 3. Results

#### 3.1. Crystal Structures of the SrLnCuTe<sub>3</sub> Series

According to the data of X-ray diffraction analysis of single crystals, the compounds SrLnCuTe<sub>3</sub> (Ln = Sm, Gd and Tb) crystallize in the orthorhombic space group *Pnma* with the structure type (ST) Eu<sub>2</sub>CuS<sub>3</sub>, and the other SrLnCuTe<sub>3</sub> members (Ln = Dy–Tm and Lu) adopt the orthorhombic space group *Cmcm* with the structure type of KZrCuS<sub>3</sub>. The crystallographic data, details of the data collections, atomic coordinates, thermal displacement parameters, bond lengths and bond angles are given in Tables 1–3 as well as S1 and S2 in the section Supplementary Material. Similar structural types were observed in the quaternary chalcogenides of the alkaline-earth elements AELnCuCh<sub>3</sub> (AE = Sr, Ba; Ch = S, Se and Te) [2,3,18,20,26,27,29–35,37–39].

**Table 1.** Main parameters of processing and refinement of the SrLnCuTe<sub>3</sub> (Ln = Sm, Gd and Tb) samples.

	SrSmCuTe <sub>3</sub>	SrGdCuTe <sub>3</sub>	SrTbCuTe <sub>3</sub>
Molecular weight	684.31	691.21	692.88
Space group		<i>Pnma</i>	
Structure type		Eu <sub>2</sub> CuS <sub>3</sub>	
Z		4	
<i>a</i> (Å)	11.4592(7)	11.3886(7)	11.3418(7)
<i>b</i> (Å)	4.3706(3)	4.3534(3)	4.3491(3)
<i>c</i> (Å)	14.4425(9)	14.4522(9)	14.4326(9)
<i>V</i> (Å <sup>3</sup> )	723.33(5)	716.53(5)	711.91(6)
$\rho_{\text{cal}}$ (g/cm <sup>3</sup> )	6.284	6.407	6.465
$\mu$ (mm <sup>-1</sup> )	30.006	31.351	32.173
Reflections measured	12811	11880	12049
Reflections independent	939	930	929
Reflections with $F_o > 4\sigma(F_o)$	779	756	711
$2\theta_{\text{max}}$ (°)	54.97	54.93	55.01
<i>h, k, l</i> limits		$-14 \leq h \leq 14; -5 \leq k \leq 5; -18 \leq l \leq 18$	
$R_{\text{int}}$	0.106	0.081	0.092
	<i>Refinement results</i>		
Number of refinement parameters		38	
$R_1$ with $F_o > 4\sigma(F_o)$	0.032	0.029	0.034
$wR_2$	0.082	0.068	0.078
<i>Goof</i>	1.108	1.050	1.002
$\Delta\rho_{\text{max}}$ (e/Å <sup>3</sup> )	1.756	1.207	1.692
$\Delta\rho_{\text{min}}$ (e/Å <sup>3</sup> )	-1.809	-1.263	-1.616
Extinction coefficient, $\epsilon$	0.0026(2)	0.0022(2)	0.0036(2)
CSD-number	2232068	2232064	2232069

The crystal structures of the SrLnCuTe<sub>3</sub> series of strontium tellurides of different structural types have both similarities and differences (Figure 1). The similarity lies in the fact that in all the SrLnCuTe<sub>3</sub> crystal structures of both structure types, the Sr<sup>2+</sup> and Ln<sup>3+</sup> cations take independent crystallographic positions. Aside from the structures of the entire SrLnCuTe<sub>3</sub> series being built by distorted [CuTe<sub>4</sub>]<sup>7-</sup> tetrahedra, they are connected by two common vertices into infinite linear chains  $\infty 1\{[Cu(Te1)1/1t(Te2)1/1t(Te3)2/2e]^{5-}\}$  and distorted octahedra [LnTe<sub>6</sub>]<sup>9-</sup> and connected by common edges and vertices into layers  $\infty 2\{[Ln(Te1)2/2(Te2)2/2(Te3)2/2]^{3-}\}$  along the [010] direction in SrLnCuTe<sub>3</sub> (Ln = Sm, Gd and Tb) adopting the structure type of Eu<sub>2</sub>CuS<sub>3</sub> and along the [100] direction in SrLnCuTe<sub>3</sub> (Ln = Sm, Gd–Tm and Lu), having the structure KZrCuS<sub>3</sub> type. The distorted

octahedra and tetrahedra also form parallel two-dimensional layers  $\infty 2\{[CuLnTe_3]^{2-}\}$  and between them, there are  $Sr^{2+}$  cations providing the three-dimensionality of the structure. While the  $Cu^+$  and  $Ln^{3+}$  cations form the same coordination polyhedra in different structural types, the  $Sr^{2+}$  cations have different coordination environments. Strontium cations in the compounds  $SrLnCuTe_3$  ( $Ln = Sm, Gd$  and  $Tb$ ) are coordinated by seven  $Te^{2-}$  anions to form the coordination polyhedron of a capped trigonal prism  $[SrTe_{6+1}]^{12-}$  with the symmetry  $mm2$ . These monocapped trigonal prisms are articulated by facets and edges to form layers  $\infty 2\{[Sr(Te1)2/2(Te2)3/3(Te3)2/2]^{4-}\}$  located parallel to the (001) plane. However, in the compounds  $SrLnCuTe_3$  ( $Ln = Dy-Tm$  and  $Lu$ ) the strontium cations are found in a trigonal-prismatic coordination environment  $[SrTe_6]^{10-}$ . The polyhedra have a local symmetry of  $\bar{6}m2$  (high symmetry coordination) and are connected by facets and form one-dimensional chains  $\infty 1\{[Sr(Te1)2/2(Te2)3/3(Te3)2/2]^{4-}\}$  along the [100] direction.

**Table 2.** Main parameters of processing and refinement of the  $SrLnCuTe_3$  ( $RE = Dy-Tm$  and  $Lu$ ) samples.

	$SrDyCuTe_3$	$SrHoCuTe_3$	$SrErCuTe_3$	$SrTmCuTe_3$	$SrLuCuTe_3$
Molecular weight	696.46	698.89	701.22	702.89	708.93
Space group			$Cmcm$		
Structure type			$KZrCuS_3$		
Z			4		
a (Å)	4.3405(3)	4.3314(3)	4.3258(3)	4.3198(3)	4.3064(3)
b (Å)	14.4298(9)	14.4179(9)	14.4123(9)	14.4037(9)	14.3879(9)
c (Å)	11.2972(7)	11.2532(7)	11.2176(7)	11.1902(7)	11.1408(7)
V (Å <sup>3</sup> )	707.54(5)	702.85(4)	699.36(6)	696.28(4)	690.28(6)
$\rho_{cal}$ (g/cm <sup>3</sup> )	6.538	6.605	6.660	6.705	6.822
$\mu$ (mm <sup>-1</sup> )	32.936	33.783	34.637	35.480	37.237
Reflections measured	7403	6637	6693	9931	6818
Reflections independent	484	484	483	482	480
Reflections with $F_o > 4\sigma(F_o)$	420	462	444	446	429
$2\theta_{max}$ (°)	54.878	54.934	54.922	54.938	55.016
$h, k, l$ limits		$-5 \leq h \leq 5; -18 \leq k \leq 18; -14 \leq l \leq 14$			
$R_{int}$	0.074	0.044	0.062	0.070	0.073
		<i>Refinement results</i>			
Number of refinement parameters			24		
$R_1$ with $F_o > 4\sigma(F_o)$	0.026	0.018	0.023	0.018	0.025
$wR_2$	0.059	0.040	0.054	0.043	0.045
$Goof$	1.055	1.109	1.102	1.079	1.088
$\Delta\rho_{max}$ (e/Å <sup>3</sup> )	1.413	1.244	1.604	0.859	1.781
$\Delta\rho_{min}$ (e/Å <sup>3</sup> )	-1.472	-1.293	-1.638	-0.906	-1.853
Extinction coefficient, $\epsilon$	0.0011(1)	0.00184(9)	0.0008(1)	0.00125(9)	0.00082(7)
CSD-number	2232062	2232065	2232063	2223070	2232066

**Table 3.** Fractional atomic coordinates and isotropic or equivalent isotropic displacement parameters of the  $SrLnCuTe_3$  series ( $Ln = Sm, Gd-Tm$  and  $Lu$ ).

Atom	$x/a$	$y/b$	$z/c$	$U_{iso}^*/U_{eq}$ (Å <sup>2</sup> )
<b>SrSmCuTe<sub>3</sub></b>				
Sr	0.26969(11)	$1/4$	0.50279(9)	0.0267(3)
Sm	0.01491(5)	$1/4$	0.74492(4)	0.0215(2)
Cu	0.24071(13)	$1/4$	0.22143(12)	0.0312(4)
Te1	0.05395(7)	$1/4$	0.11132(6)	0.0217(2)
Te2	0.41676(7)	$1/4$	0.10364(6)	0.0226(2)
Te3	0.26215(7)	$1/4$	0.83011(6)	0.0212(2)

Table 3. Cont.

Atom	$x/a$	$y/b$	$z/c$	$U_{iso}^*/U_{eq} (\text{\AA}^2)$
<b>SrGdCuTe<sub>3</sub></b>				
Sr	0.26663(9)	1/4	0.50313(8)	0.0243(3)
Gd	0.01350(4)	1/4	0.74611(3)	0.0188(2)
Cu	0.24205(12)	1/4	0.22125(11)	0.0288(4)
Te1	0.05418(6)	1/4	0.11125(5)	0.0190(2)
Te2	0.42077(6)	1/4	0.10495(5)	0.0196(2)
Te3	0.26121(6)	1/4	0.83009(5)	0.0186(2)
<b>SrTbCuTe<sub>3</sub></b>				
Sr	0.26394(11)	1/4	0.50354(9)	0.0247(3)
Tb	0.01132(5)	1/4	0.74680(4)	0.0200(2)
Cu	0.24340(14)	1/4	0.22102(12)	0.0281(4)
Te1	0.05508(7)	1/4	0.11105(6)	0.0190(3)
Te2	0.42398(7)	1/4	0.10569(6)	0.0196(3)
Te3	0.25953(7)	1/4	0.82978(6)	0.0183(2)
<b>SrDyCuTe<sub>3</sub></b>				
Sr	0	0.75369(9)	1/4	0.0313(4)
Dy	0	0	0	0.0245(2)
Cu	0	0.47094(13)	1/4	0.0301(4)
Te1	0	0.07951(6)	1/4	0.0217(3)
Te2	0	0.35881(4)	0.06439(5)	0.0253(2)
<b>SrHoCuTe<sub>3</sub></b>				
Sr	0	0.75402(7)	1/4	0.0258(2)
Ho	0	0	0	0.0194(2)
Cu	0	0.47067(9)	1/4	0.0269(3)
Te1	0	0.07945(4)	1/4	0.0179(2)
Te2	0	0.35906(3)	0.06332(4)	0.0192(2)
<b>SrErCuTe<sub>3</sub></b>				
Sr	0	0.75401(9)	1/4	0.0248(3)
Er	0	0	0	0.0193(2)
Cu	0	0.47055(12)	1/4	0.0273(4)
Te1	0	0.07917(5)	1/4	0.0183(2)
Te2	0	0.35928(4)	0.06242(5)	0.0190(2)
<b>SrTmCuTe<sub>3</sub></b>				
Sr	0	0.75437(7)	1/4	0.0230(3)
Tm	0	0	0	0.0176(2)
Cu	0	0.47054(9)	1/4	0.0254(3)
Te1	0	0.07905(4)	1/4	0.0164(2)
Te2	0	0.35962(3)	0.06173(4)	0.0172(2)
<b>SrLuCuTe<sub>3</sub></b>				
Sr	0	0.75465(9)	1/4	0.0234(3)
Lu	0	0	0	0.0173(2)
Cu	0	0.47013(12)	1/4	0.0261(4)
Te1	0	0.07884(6)	1/4	0.0169(2)
Te2	0	0.36010(4)	0.06020(5)	0.0177(2)

Thus, the three-dimensional crystal structure of SrLnCuTe<sub>3</sub> (Ln = Sm, Gd and Tb) and SrLnCuTe<sub>3</sub> (Ln = Dy–Tm and Lu) is resulting from two-dimensional layers formed by octahedra and tetrahedra in the *ac* and *bc* planes, accordingly, these layers are separated by naked dimer ribbons or by alternating polymeric chains formed in turn by monocapped trigonal prisms and naked trigonal prisms, respectively (Figure 1).

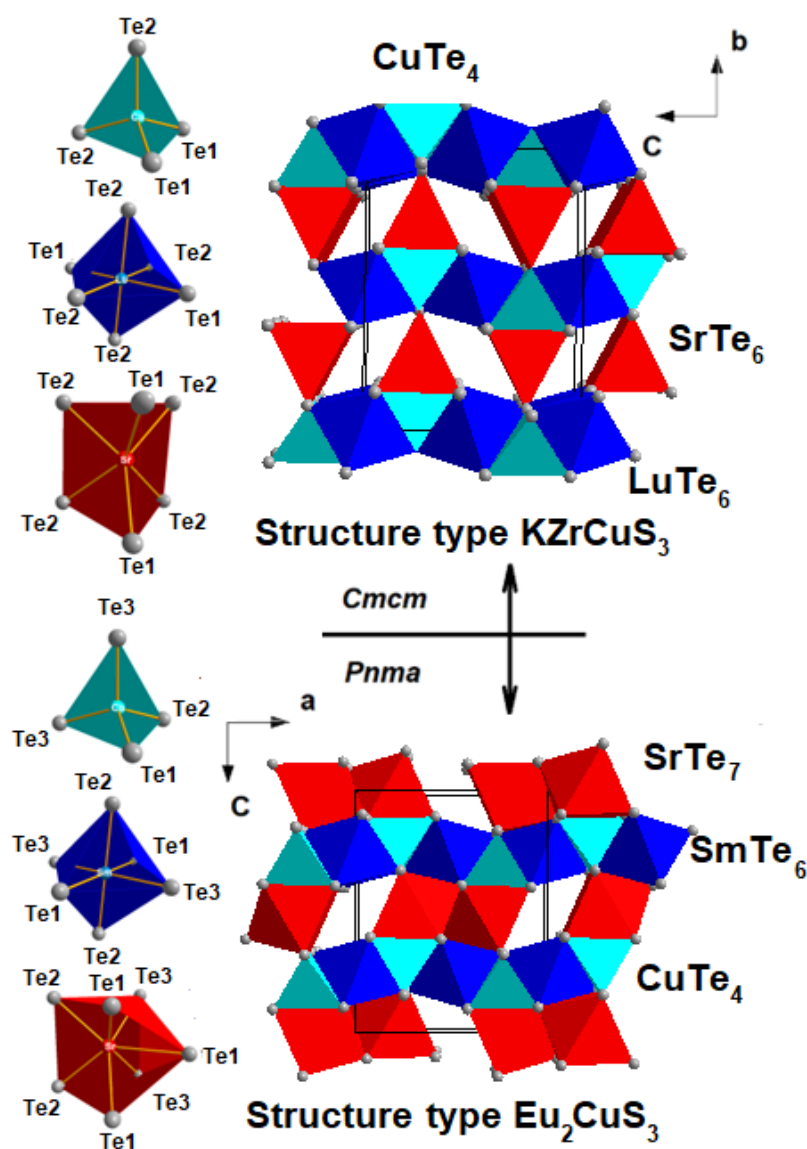


**Figure 1.** View at the orthorhombic crystal structures of the  $\text{SrLnCuTe}_3$  series ( $\text{Ln} = \text{Dy–Tm}$  and  $\text{Lu}$ ) with the space group  $Cmcm$  (top view), and the  $\text{SrLnCuTe}_3$  series ( $\text{Ln} = \text{Sm, Gd}$  and  $\text{Tb}$ ) of the space group  $Pnma$  (bottom view), along the  $a$ -axis and the  $b$ -axis, respectively, together with the telluride coordination polyhedra formed around metal cations.

As the radius of  $r_i(\text{Ln}^{3+})$  decreases, the parameters of the unit cell also decrease (notably, the values of the unit-cell parameters  $b$ ,  $c$  and  $a$  in space group  $Pnma$  correspond to  $a$ ,  $b$  and  $c$  in space group  $Cmcm$ ), the volumes of the unit cells decrease from  $723.33(5) \text{ \AA}^3$  for  $\text{SrSmCuTe}_3$  to  $690.28(6) \text{ \AA}^3$  for  $\text{SrLuCuTe}_3$  (Tables 1 and 2), as well as the distance  $d(\text{Ln–Te})$  in the interval  $3.1161(9)–3.0075(5) \text{ \AA}$  (Figure 2 and Table S1 in the Supplementary Material), that result in a decrease in coordination saturation for  $\text{Ln}^{3+}$ . Since the distorted octahedra  $[\text{LnTe}_6]^{9-}$  in all compounds are connected with tetrahedra  $[\text{CuTe}_4]^{7-}$  to form two-dimensional layers  $\infty 2\{[\text{CuLnTe}_3]^{2-}\}$ , a decrease in the cation radius  $r_i(\text{Ln}^{3+})$  results in crystal-chemical compression of the layers. The change in the strontium coordination polyhedron from a monocapped trigonal prism  $[\text{SrTe}_{6+1}]^{12-}$  to the trigonal prism  $[\text{SrTe}_6]^{9-}$  manifests in changing the structure type from  $\text{Eu}_2\text{CuS}_3$  to  $\text{KZrCuS}_3$  and space group from  $Pnma$  to  $Cmcm$  (Figure 1). Similar transformations were observed for  $\text{AELnCuCh}_3$  ( $\text{AE} = \text{Ba, Sr, Eu}$ ;  $\text{Ch} = \text{S, Se}$ ) already [20,30,31,33,35,39,41,44,45].

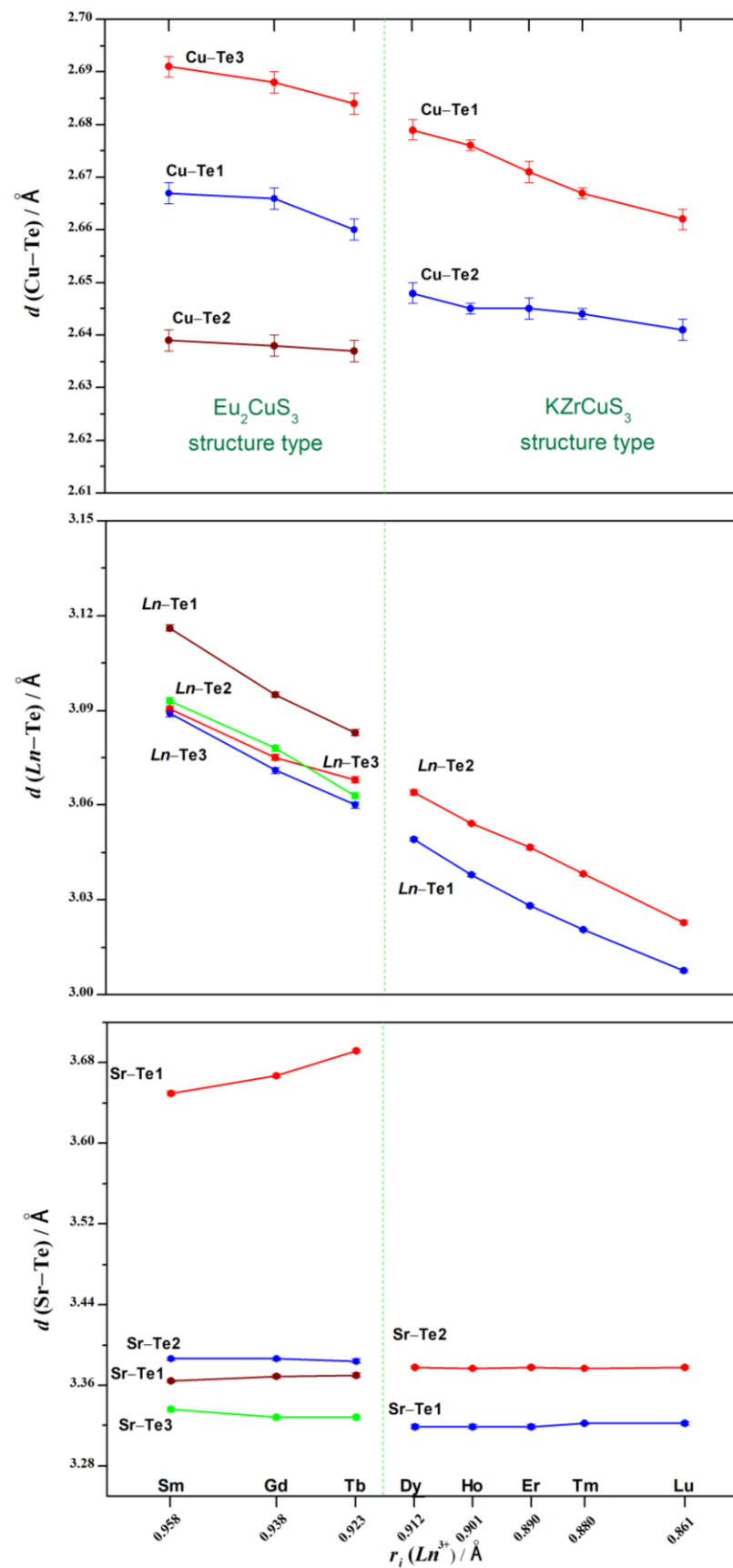
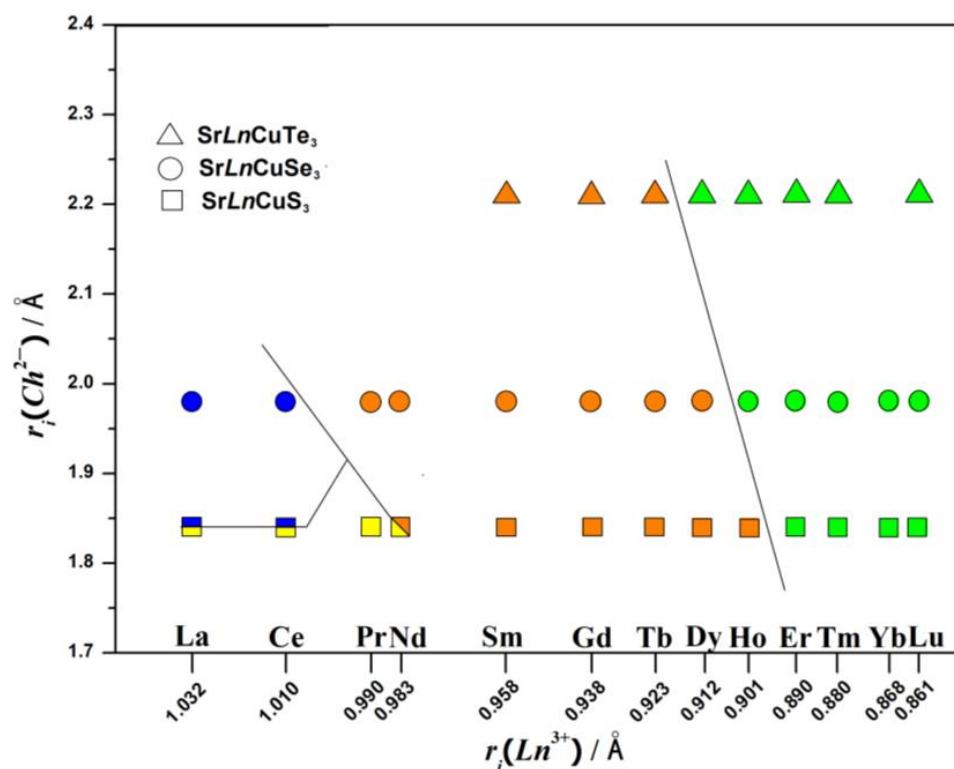


Figure 2. The M-Te distances in both structures of the  $SrLnCuTe_3$  series ( $Ln = Sm, Gd-Tm$  and  $Lu$ ).

In the  $\text{SrLnCuTe}_3$  ( $Ln = \text{Sm, Gd and Tb}$ ) structures of the structure type  $\text{Eu}_2\text{CuS}_3$ , the coordination polyhedron  $[\text{SrTe}_{6+1}]^{12-}$  six distances of  $d(\text{Sr}-\text{Te})$  are shorter than 3.39 Å, and the seventh distance  $d(\text{Sr}-\text{Te})$  gradually increases: 3.650(2) Å ( $\text{SrSmCuTe}_3$ )  $\rightarrow$  3.667(2) Å ( $\text{SrGdCuTe}_3$ )  $\rightarrow$  3.692 Å ( $\text{SrTbCuTe}_3$ ) (Table S1, Figure 2). A similar trend was observed for the isostructural compounds  $\text{EuLnCuS}_3$  [46] and  $\text{SrLnCuS}_3$  [30,40]. In the structures for  $\text{SrLnCuTe}_3$  ( $Ln = \text{Dy-Tm and Lu}$ ) of the structure type  $\text{KZrCuS}_3$ , the cations  $\text{Sr}^{2+}$  have six distances  $d(\text{Sr}-\text{Te})$ , being shorter than 3.38 Å and two additional anions  $\text{Te}^{2-}$  ( $2 \times 3.905(2)$  Å ( $\text{SrDyCuTe}_3$ ),  $2 \times 3.8843(9)$  Å ( $\text{SrHoCuTe}_3$ ),  $2 \times 3.866(2)$  Å ( $\text{SrErCuTe}_3$ ),  $2 \times 3.8550(8)$  Å ( $\text{SrTmCuTe}_3$ ),  $2 \times 3.830(2)$  Å ( $\text{SrLuCuTe}_3$ ). The seventh and the eighth telluride anion are not included in the coordination of  $\text{Sr}^{2+}$  due to the very weak interactions.

All currently known compounds of formula  $\text{SrLnCuCh}_3$  with  $Ch = \text{S}$  [30,33,39], Se [33,35] and Te [this work] are shown in Figure 3. There, the ionic radii of the divalent anions ( $Ch^{2-}$ ) are plotted against the ionic radii of the cations of the trivalent lanthanoid cations ( $Ln^{3+}$ ). The lines represent virtual boundaries between each type of structure and have been arbitrarily added to the diagram to provide a visual breakline between modifications. The chalcogenides  $\text{SrLnCuCh}_3$  are isostructural. When transiting from sulfur to tellurium, the anion sublattice expands ( $r(\text{S}^{2-}) = 1.84$  Å,  $r(\text{Se}^{2-}) = 1.98$  Å,  $r(\text{Te}^{2-}) = 2.21$  Å [47]). The change of the structure type from  $\text{Eu}_2\text{CuS}_3$  to  $\text{KZrCuS}_3$  in sulfides occurs at the Y/Er boundary [39,45]; in selenides, it is found at the Dy/Ho boundary [33,41]; and in tellurides, it meets the Tb/Dy boundary (Figure 3). Thus, the larger the chalcogenide radius, the earlier the change of the structure type and the space group from  $Pnma$  to  $Cmcm$  in the  $\text{SrLnCuCh}_3$  series of quaternary chalcogenides takes place.



**Figure 3.** Structure field diagram of  $\text{SrLnCuCh}_3$  chalcogenides with  $Ch = \text{S}$  [39,45], Se [33,41] and Te [this work]. Description: color background corresponds to a defined structure type (yellow:  $\text{BaLaCuS}_3$ , blue:  $\text{Ba}_2\text{MnS}_3$ , green:  $\text{KZrCuS}_3$ , orange:  $\text{Eu}_2\text{CuS}_3$ ).

The barium compounds  $\text{BaLnCuTe}_3$  were previously discovered as quaternary tellurides [2,3,20,21]. In these tellurides, the change of space group occurs on the lightest rare-earth elements  $\text{BaLaCuTe}_3$  ( $Pnma$ )/ $\text{BaPrCuTe}_3$  ( $Cmcm$ ) [3,20]. The ionic radius of barium  $r_i(\text{Ba}^{2+}) = 1.38$  Å is larger than that one of strontium  $r_i(\text{Sr}^{2+}) = 1.21$  Å [47]. The smaller

the radius of the alkaline-earth cation, the smaller the number of compounds crystallizing in the space group  $Cmcm$ , and the cations  $AE^{2+}$  later become six-fold coordinated.

It can be assumed that in the quaternary strontium tellurides, the replacement of monovalent copper ( $r_i(\text{Cu}^+) = 0.60 \text{ \AA}$  [47]) with silver ( $r_i(\text{Ag}^+) = 1.00 \text{ \AA}$  [47]) will result in the change of the space group in compounds containing rare-earth elements of the very beginning of the lanthanoid series or as in the case of the barium tellurides  $\text{BaLnAgTe}_3$  [3,20,21], all the series will crystallize in  $Cmcm$ .

We also compared the distortion degree to the  $[\text{CuTe}_4]^{7-}$  coordination polyhedra in the crystalline  $\text{SrLnCuTe}_3$  structure series. Deviations from the symmetry of tetrahedra  $[\text{CuTe}_4]^{7-}$  can be affected by distances  $d(\text{Cu—Te})$ ,  $d(\text{Te}\cdots\text{Te})$ , angles  $\angle(\text{Te—Cu—Te})$ . To estimate the degree of distortion for the polyhedra  $[\text{CuTe}_4]^{7-}$ , the distortion coefficients were calculated using the methods proposed in [48,49],

$$DI(\text{TeCuTe}) = \frac{\left(\sum_{i=1}^6 |\text{TeCuTe}_i - \text{TeCuTe}_m|\right)}{(6 \cdot \text{TeCuTe}_m)},$$

where  $DI$  is a distortion index,  $\text{TeCuTe}_i$  is the  $i$ -tetrahedral angle (Table S2),  $\text{TeCuTe}_m$  is an angle of a regular tetrahedron that equals  $109.47^\circ$ .

$$D(\text{CuTe}) = \frac{\left(\sum_{i=1}^4 |\text{CuTe}_i - \text{CuTe}_m|\right)}{(4 \cdot \text{CuTe}_m)},$$

$$D(\text{TeTe}) = \frac{\left(\sum_{i=1}^6 |\text{TeTe}_i - \text{TeTe}_m|\right)}{(6 \cdot \text{TeTe}_m)},$$

where  $\text{CuTe}_i$  and  $\text{TeTe}_i$  refer to the individual values (Table S1),  $\text{CuTe}_m$  and  $\text{TeTe}_m$  are the theoretic bond lengths for a coordination number of 4, equal to  $2.81 \text{ \AA}$  and  $4.42 \text{ \AA}$ , respectively, calculated from the values of the ionic radii  $r_i(\text{Cu}^+)$  and  $r_i(\text{Te}^{2-})$  [47].

In the series of the  $\text{SrLnCuTe}_3$  compounds, a decrease in the deviation of bond angles  $\angle(\text{Te—Cu—Te})$  from the symmetric coordination and the formation of the most symmetric structure  $[\text{CuTe}_4]^{7-}$  in transition to the compounds  $\text{SrLnCuTe}_3$ , containing  $\text{Ln}^{3+}$  with a small ionic radius are observed (Table 4). However, there is an increase in the degree of weakening of the bonds  $d(\text{Cu—Te})$ . Distortions are more distinct in distances  $d(\text{Cu—Te})$  than in  $d(\text{Te}\cdots\text{Te})$  and  $\angle(\text{Te—Cu—Te})$ . Probably, the local character of distortions in the  $d(\text{Cu—Te})$  bonds does not affect the general character of the symmetry within the structure.

**Table 4.** The degree of distortion  $DI$  of tetrahedra for the compounds  $\text{SrLnCuTe}_3$  ( $\text{Ln} = \text{Sm}, \text{Gd–Tm}$  and  $\text{Lu}$ ).

Compound	Structure Type	$DI(\text{Te—Cu—Te})$	$DI(\text{Cu—Te})$	$DI(\text{Te}\cdots\text{Te})$	$\tau_4$
$\text{SrSmCuTe}_3$	$\text{Eu}_2\text{CuS}_3$	0.0214	0.0491	0.0157	0.955
$\text{SrGdCuTe}_3$	$\text{Eu}_2\text{CuS}_3$	0.0208	0.0499	0.0155	0.957
$\text{SrTbCuTe}_3$	$\text{Eu}_2\text{CuS}_3$	0.0192	0.0512	0.0152	0.961
$\text{SrDyCuTe}_3$	$\text{KZrCuS}_3$	0.0182	0.0521	0.0161	0.979
$\text{SrHoCuTe}_3$	$\text{KZrCuS}_3$	0.0174	0.0533	0.0173	0.980
$\text{SrErCuTe}_3$	$\text{KZrCuS}_3$	0.0164	0.0541	0.0181	0.981
$\text{SrTmCuTe}_3$	$\text{KZrCuS}_3$	0.0155	0.0550	0.0191	0.982
$\text{SrLuCuTe}_3$	$\text{KZrCuS}_3$	0.0140	0.0564	0.0205	0.984

The tetracoordinated environment can also be characterized using the  $\tau_4$ -descriptor [50]. The values of  $\tau_4$  are the following: for ideal tetrahedral structures it is 1.00, for trigonal-pyramidal structures 0.85, for seesaw structures 0.64–0.07 and for perfect square planar structures 0.00. The  $\tau_4$  values of the tellurides  $\text{SrLnCuTe}_3$  ( $\text{Ln} = \text{Sm}, \text{Gd–Tm}$  and  $\text{Lu}$ ) of both structure types range from 0.955 to 0.984 (Table 4 and Figure 4), indicating that the coordination geometry around  $\text{Cu}^+$  is distorted by 10–30% from an ideal tetrahedron to a

trigonal pyramidal structure. A greater distortion of tetrahedra is observed in compounds crystallizing in space group  $Pnma$  ( $\tau_4$  varies from 0.955 to 0.961) than in  $Cmcm$  ( $\tau_4$  varies from 0.979 to 0.996) (Figure 4). A jump in the  $\tau_4$ -descriptor occurs at the boundary of the change of structure types. As  $r_i(Ln^{3+})$  decreases, a decrease in the distortion of the tetrahedron is observed.

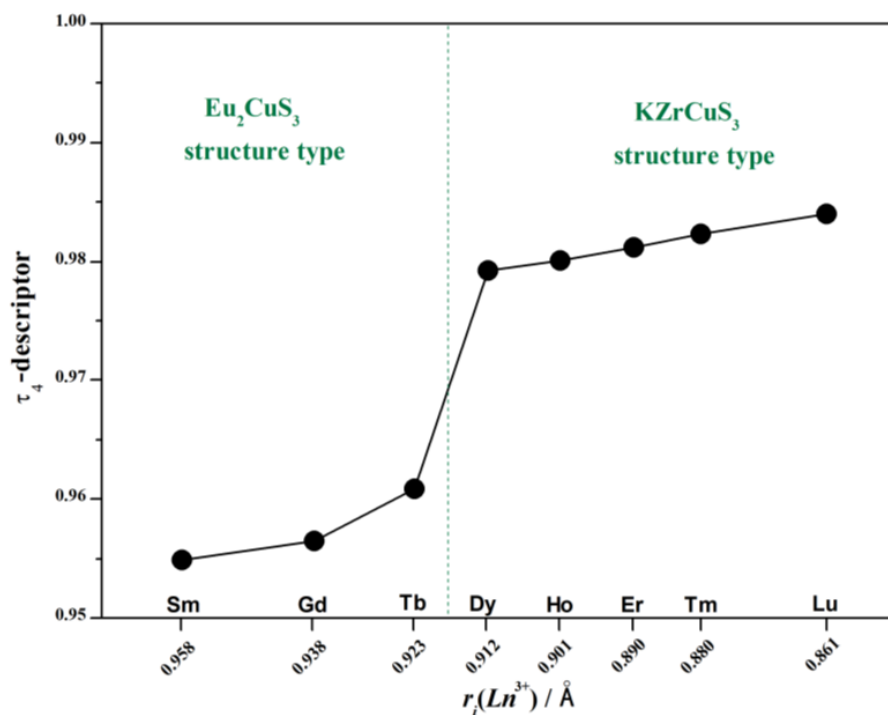


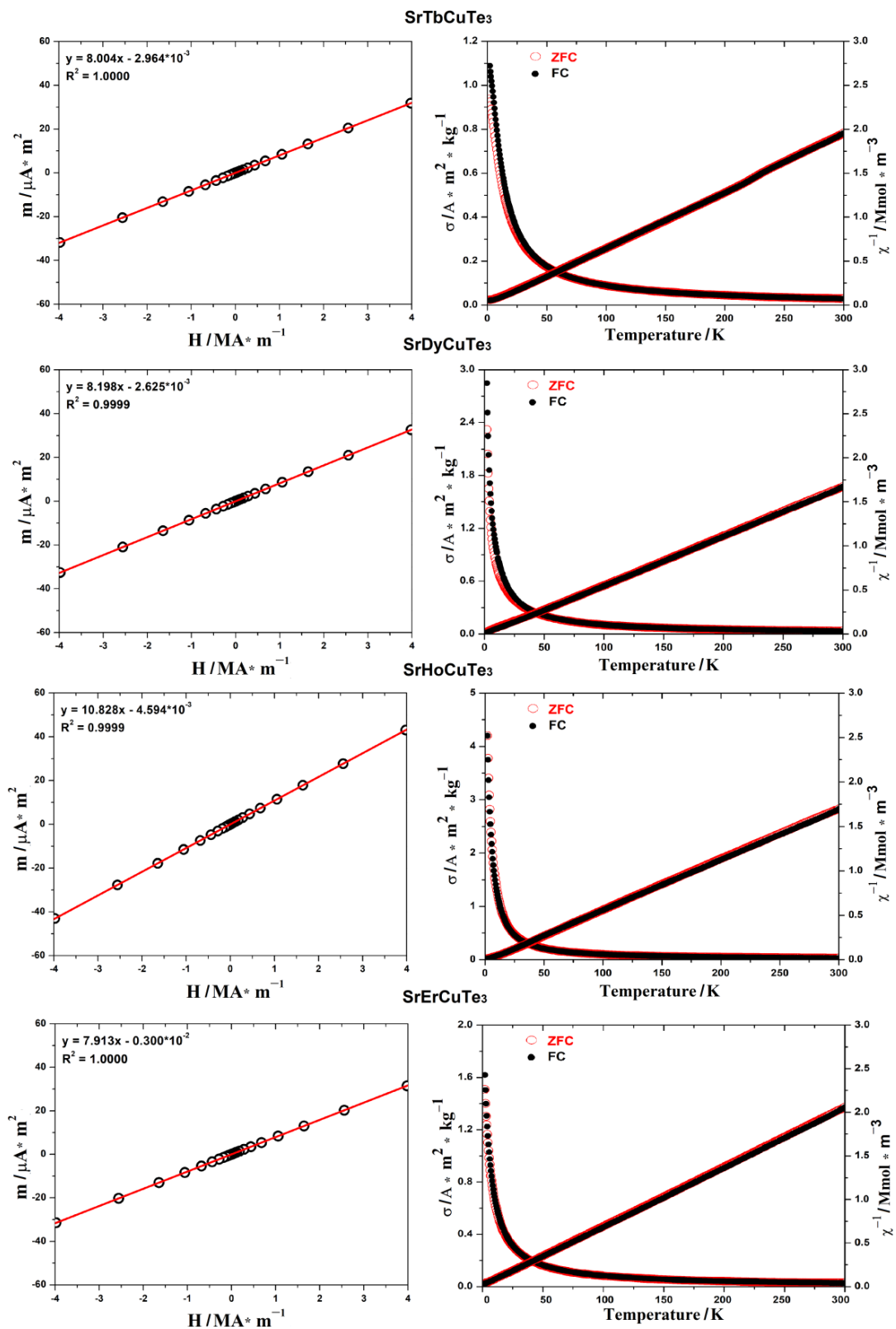
**Figure 4.** Calculated  $\tau_4$ -descriptor values for the  $[CuTe_4]^{7-}$  polyhedra in the crystal structures of the  $SrLnCuTe_3$  series.

### 3.2. Magnetic Properties of the $SrLnCuTe_3$ Series ( $Ln = Tb-Er$ )

The temperature dependencies of the sample magnetizations have a shape characteristic of paramagnets (Figure 5). They are described with high accuracy by the Curie–Weiss law at temperature ranges from 100 to 300 K. The Curie constants  $C$  calculated from these dependencies, the effective magnetic moments  $\mu$  and the Curie–Weiss temperatures  $\theta$  are shown in Table 5. The values of  $C$  and  $\mu$  are very close to the theoretical ones for the corresponding independent magnetic cations. The values of the Curie–Weiss constants  $\theta$  in all the samples are positive, which indicates the ferromagnetic nature of the interaction of magnetic  $Ln^{3+}$  cations ( $Ln = Tb-Er$ ) with a decrease in temperature, however, Curie temperatures are below 2 K. The dependences of magnetization on the external magnetic field are linear at a temperature of 300 K. The parameters  $C$  and  $\mu$  calculated from them are also listed in Table 5.

Magnetic field dependencies at 2 K calculated with reference to one formula unit are shown in Figure 6. Their view is characteristic of a ferromagnet slightly above the Curie temperature, where saturation is not reached up to very strong fields. Theoretically, the saturated magnetization for  $Tb^{3+}$  and  $Er^{3+}$  cations is  $9 \mu_B$ , and for  $Dy^{3+}$  and  $Ho^{3+}$   $10 \mu_B$ .

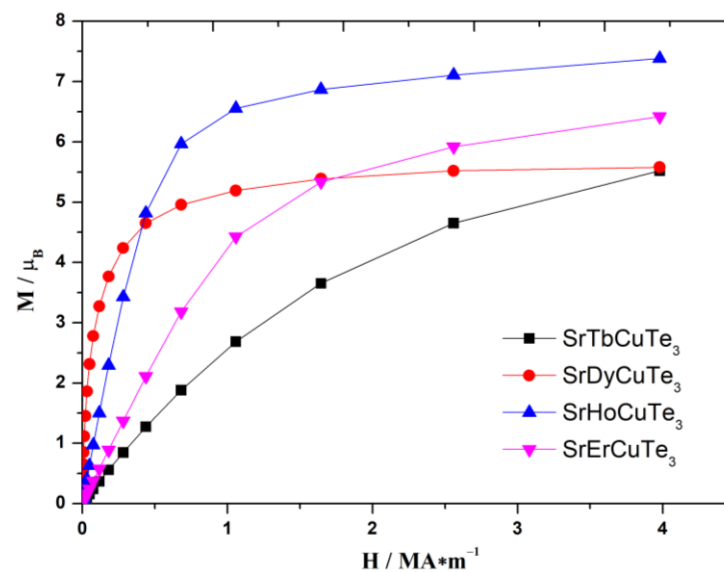
The magnetization curve of  $SrDyCuTe_3$  shows such a strong tendency to saturation that it can be assumed that there occurs ferromagnetic ordering; however, the temperature dependencies of the magnetization do not provide reasons to claim that the transition to the ferromagnetic state at 2 K really took place. The value of the magnetic moment per one formula unit is almost two times less than the moment of the free cation  $Dy^{3+}$  ( $10 \mu_B$ ). The cause of this behavior remains unclear.



**Figure 5.** Field-dependent magnetic moment at 300 K (left), temperature-dependent specific magnetization and reciprocal magnetic susceptibility at 500 kOe (right) of  $SrLnCuTe_3$  samples with  $Ln = Tb$ – $Er$ . The measurements of low-temperature magnetization were performed in the zero-field cooled (ZFC) and nonzero-field cooled (FC) modes.

**Table 5.** Magnetic characteristics for the SrLnCuTe<sub>3</sub> series (Ln = Tb–Er).

	SrTbCuTe <sub>3</sub>	SrDyCuTe <sub>3</sub>	SrHoCuTe <sub>3</sub>	SrErCuTe <sub>3</sub>
Space group	<i>Pnma</i>		<i>Cmcm</i>	
Structure type	Eu <sub>2</sub> CuS <sub>3</sub>		KZrCuS <sub>3</sub>	
Experimental $\mu_{300\text{ K}}$ ( $\mu_B$ )	9.57	10.34	10.49	9.33
Experimental $\mu_{2-300\text{ K}}$ ( $\mu_B$ )	9.80	10.63	10.59	9.64
Calculated $\mu$ ( $\mu_B$ )	9.721	10.646	10.607	9.581
Experimental $C_{300\text{ K}}$ ( $\text{K}\cdot\text{m}^3\cdot\text{kmol}^{-1}$ )	0.144	0.168	0.173	0.137
Experimental $C_{2-300\text{ K}}$ ( $\text{K}\cdot\text{m}^3\cdot\text{kmol}^{-1}$ )	0.151	0.178	0.176	0.146
Calculated $C$ ( $\text{K}\cdot\text{m}^3\cdot\text{kmol}^{-1}$ )	0.149	0.178	0.177	0.144
$\theta_p$ (K)	5.2	2.9	1.1	0.5

**Figure 6.** Magnetization curves of SrLnCuTe<sub>3</sub> samples with Ln = Tb–Er at 2 K.

#### 4. Conclusions

For the first time, there are eight new layered heterometallic quaternary strontium tellurides SrLnCuTe<sub>3</sub> (Ln = Sm, Gd–Tm and Lu). Single crystals were synthesized by the ampoule method from stoichiometric mixtures of the initial elements Sr, Ln, Cu and Te in the presence of CsI as halogenide flux. It is established that orthorhombic tellurides SrLnCuTe<sub>3</sub> (Ln = Sm, Gd and Tb) crystallize in the space group *Pnma* with the structure type of Eu<sub>2</sub>CuS<sub>3</sub>, whereas SrLnCuTe<sub>3</sub> (Ln = Dy–Tm and Lu), the space group *Cmcm* with the structure type KZrCuS<sub>3</sub>, is formed. It is shown that both types of crystal structures show octahedra around Ln<sup>3+</sup> and tetrahedra around Cu<sup>+</sup> of Te<sup>2-</sup> anions as coordination spheres, but differ in the coordination of the alkaline-earth element. In the SrLnCuTe<sub>3</sub> compounds (Ln = Dy–Tm and Lu), Sr<sup>2+</sup> is characterized by highly symmetric trigonal-prismatic coordination, while in the compounds SrLnCuTe<sub>3</sub> (Ln = Sm, Gd and Tb), a less symmetrical capped trigonal prism occurs. Both structures are formed from layers that are separated by either dimeric ribbons formed by the capped trigonal prisms or alternating chains formed by the naked prisms. The distortion of the polyhedron [CuTe<sub>4</sub>]<sup>7-</sup> is compared for the entire SrLnCuTe<sub>3</sub> series using the t<sub>4</sub>-descriptor for four coordinated ions. It is established that the lowest degree of distortion of tetrahedra is characteristic of SrLuCuTe<sub>3</sub>. The tellurides SrLnCuTe<sub>3</sub> (Ln = Tb–Er) of both structure types are paramagnetic in the temperature range from 2 to 300 K and are supposed to have ferromagnetic Curie temperatures below 2 K. The experimental magnetic characteristics are consistent with the corresponding calculated parameters.

**Supplementary Materials:** The following supporting information can be downloaded at: <https://www.mdpi.com/article/10.3390/cryst13020291/s1>.

**Author Contributions:** Conceptualization, A.V.R. and M.V.G.; software, A.V.R. and M.V.G.; validation, A.V.R.; formal analysis, M.V.G., M.S.M. and R.J.C.L.; investigation, M.V.G.; resources, T.S.; data curation, A.V.R., T.S. and M.V.G.; writing—original draft preparation, A.A.G., A.V.R., T.S. and M.V.G.; writing—review and editing, A.V.R., M.S.M., A.A.G. and T.S.; visualization, M.S.M., A.A.G. and M.V.G.; project administration, A.V.R.; funding acquisition, M.V.G. and A.V.E. All authors have read and agreed to the published version of the manuscript.

**Funding:** The research was supported by the Tyumen region within the framework of the grant agreement in the form of a grant to non-profit organizations no. 89-don dated 7 December 2020.

**Institutional Review Board Statement:** Not applicable.

**Informed Consent Statement:** Not applicable.

**Data Availability Statement:** All the data supporting the conclusions is included within the manuscript and is available on request from the corresponding authors.

**Acknowledgments:** We gratefully acknowledge the help of Björn Blaschkowski for the magnetic measurements and Jean-Louis Hoslauer for the PXRD investigations, both at the Institute for Inorganic Chemistry at the University of Stuttgart.

**Conflicts of Interest:** The authors declare no conflict of interest.

## References

1. Pal, K.; Xia, Y.; Shen, J.; He, J.; Luo, Y.; Kanatzidis, M.G.; Wolverton, C. Accelerated discovery of a large family of quaternary chalcogenides with very low lattice thermal conductivity. *Comput. Mater.* **2021**, *7*, 82. [\[CrossRef\]](#)
2. Ishtiyak, M.; Jana, S.; Karthikeyan, R.; Mamindla, R.; Tripathy, B.; Malladi, S.K.; Niranjana, M.; Prakash, J. Syntheses of five new layered quaternary chalcogenides SrScCuSe<sub>3</sub>, SrScCuTe<sub>3</sub>, BaScCuSe<sub>3</sub>, BaScCuTe<sub>3</sub>, and BaScAgTe<sub>3</sub>: Crystal structures, thermoelectric properties, and electronic structures. *Inorg. Chem. Front.* **2021**, *8*, 4086–4101. [\[CrossRef\]](#)
3. Yang, Y.; Ibers, J.A. Synthesis and characterization of a series of quaternary chalcogenides BaLnMQ<sub>3</sub> (Ln = rare earth, M = coinage metal, Q = Se or Te). *J. Solid State Chem.* **1999**, *147*, 366–371. [\[CrossRef\]](#)
4. Mansuetto, M.F.; Keane, P.M.; Ibers, J.A. Synthesis and Structures of the New Group IV Chalcogenides NaCuTiS<sub>3</sub> and NaCuZrQ<sub>3</sub> (Q = S, Se, Te). *J. Solid State Chem.* **1993**, *105*, 580–587. [\[CrossRef\]](#)
5. Mansuetto, M.F.; Keane, P.M.; Ibers, J.A. Synthesis, structure, and conductivity of the new group IV chalcogenides, KCuZrQ<sub>3</sub> (Q = S, Se, Te). *J. Solid State Chem.* **1992**, *101*, 257–264. [\[CrossRef\]](#)
6. Huang, F.Q.; Ibers, J.A. Syntheses, Structures, and Theoretical Study of LaCuSTe and SmCuSTe. *Inorg. Chem.* **1999**, *38*, 5978–5983. [\[CrossRef\]](#)
7. Babo, J.-M.; Albrecht-Schmitt, T.E. Ce<sub>2</sub>AgYb<sub>5/3</sub>Se<sub>6</sub>, La<sub>2</sub>CuErTe<sub>5</sub>, and Ce<sub>2</sub>CuTmTe<sub>5</sub>: Three new quaternary interlanthanide chalcogenides. *J. Solid State Chem.* **2013**, *197*, 414–419. [\[CrossRef\]](#)
8. Patschke, R.; Brazis, P.; Kannewurf, C.R.; Kanatzidis, M.G. Cu<sub>0.66</sub>EuTe<sub>2</sub>, KCu<sub>2</sub>EuTe<sub>4</sub>, and Na<sub>0.2</sub>Ag<sub>2.8</sub>EuTe<sub>4</sub>: Compounds with modulated square Te nets. *J. Mater. Chem.* **1999**, *9*, 2293–2296. [\[CrossRef\]](#)
9. Patschke, R.; Heising, J.; Kanatzidis, M.; Brazis, P.; Kannewurf, C.R. KCuCeTe<sub>4</sub>: A New Intergrowth Rare Earth Telluride with an Incommensurate Superstructure Associated with a Distorted Square Net of Tellurium. *Chem Mater.* **1998**, *10*, 695–697. [\[CrossRef\]](#)
10. Babo, J.-M.; Choi, E.S.; Albrecht-Schmitt, T.E. Synthesis, structure, magnetism, and optical properties of Cs<sub>2</sub>Cu<sub>3</sub>DyTe<sub>4</sub>. *Inorg. Chem.* **2012**, *51*, 11730–11735. [\[CrossRef\]](#)
11. Malliakas, C.D.; Kanatzidis, M.G. Charge density waves in the square nets of tellurium of AMRETe<sub>4</sub> (A = K, Na; M = Cu, Ag; RE = La, Ce). *J. Am. Chem. Soc.* **2007**, *129*, 10675–10677. [\[CrossRef\]](#) [\[PubMed\]](#)
12. Pal, K.; Xia, Y.; He, J.; Wolverton, C. High thermoelectric performance in BaAgYTe<sub>3</sub> via low lattice thermal conductivity induced by bonding heterogeneity. *Phys. Rev. Mater.* **2019**, *3*, 085402. [\[CrossRef\]](#)
13. Pal, K.; Hua, X.; Xia, Y.; Wolverton, C. Unraveling the structure-valence-property relationships in AMM'Q<sub>3</sub> chalcogenides with promising thermoelectric performance. *ACS Appl. Energy Mater.* **2019**, *3*, 2110–2119. [\[CrossRef\]](#)
14. Cody, J.A.; Ibers, J.A. Uranium Tellurides: New One- and Two-Dimensional Compounds CsUTe<sub>6</sub>, CsTiUTe<sub>5</sub>, Cs<sub>8</sub>Hf<sub>5</sub>UTe<sub>30.6</sub>, and CsCuUTe<sub>3</sub>. *Inorg. Chem.* **1995**, *34*, 3165–3172. [\[CrossRef\]](#)
15. Babo, J.-M.; Strobel, S.; Schleid, T. Syntheses and Crystal Structures of CsCuNd<sub>2</sub>Se<sub>4</sub> and CsCuGd<sub>2</sub>Te<sub>4</sub>: Two Non-Isotypical Cesium Copper Lanthanide Chalcogenides with ∞1{[CuCh<sub>3</sub>]5-} Chains of Vertex-Shared [CuCh<sub>4</sub>]7- Tetrahedra. *Z. Anorg. Allg. Chem.* **2010**, *636*, 349–355. [\[CrossRef\]](#)
16. Babo, J.-M.; Schleid, T. CsCu<sub>2</sub>Sc<sub>3</sub>Te<sub>6</sub> and CsCuY<sub>2</sub>Te<sub>4</sub>: Two new quaternary cesium copper rare-earth metal tellurides. *Solid State Sci.* **2010**, *12*, 238–245. [\[CrossRef\]](#)

17. Huang, F.Q.; Ibers, J.A. Syntheses and Structures of the Quaternary Copper Tellurides  $K_3Ln_4Cu_5Te_{10}$  ( $Ln = Sm, Gd, Er$ ),  $Rb_3Ln_4Cu_5Te_{10}$  ( $Ln = Nd, Gd$ ), and  $Cs_3Gd_4Cu_5Te_{10}$ . *J. Solid State Chem.* **2001**, *160*, 409–414. [[CrossRef](#)]
18. Huang, F.Q.; Choe, W.; Lee, S.; Chu, J.S. Syntheses and Crystal Structures of Three Copper Tellurides:  $BaDyCuTe_3$ ,  $K_{1.5}Dy_2Cu_{2.5}Te_5$ , and Acentric  $K_{0.5}Ba_{0.5}DyCu_{1.5}Te_3$ . *Chem. Mater.* **1998**, *10*, 1320–1326. [[CrossRef](#)]
19. Meng, C.-Y.; Chen, H.; Wan, P.; Chen, L. Syntheses, Structures, and Magnetic and Thermoelectric Properties of Double-Tunnel Tellurides:  $A_xRE_2Cu_{6-x}Te_6$  ( $A = K-Cs$ ;  $RE = La-Nd$ ). *Chem. Mater.* **2011**, *23*, 4910–4919. [[CrossRef](#)]
20. Koscielski, L.A.; Ibers, J.A. The structural chemistry of quaternary chalcogenides of the type  $AMM'Q_3$ . *Z. Anorg. Allg. Chem.* **2012**, *638*, 2585–2593. [[CrossRef](#)]
21. Eickmeier, K.; Poschkamp, R.; Dronskowski, R.; Steinberg, S. Exploring the impact of lone pairs on the structural features of alkaline-earth ( $A$ ) transition-metal ( $M, M'$ ) chalcogenides ( $Q$ )  $AMM'Q_3$ . *Eur. J. Inorg. Chem.* **2022**, *28*, e202200360. [[CrossRef](#)]
22. Patschke, R.; Brazis, P.; Kannewurf, C.R.; Kanatzidis, M.  $Rb_2Cu_3CeTe_5$ : A quaternary semiconducting compound with a two-dimensional polytelluride framework. *J. Mater. Chem.* **1998**, *8*, 2587–2589. [[CrossRef](#)]
23. Pell, M.A.; Ibers, J.A. Synthesis and structure of  $TiCuTiTe_3$ . *J. Alloys Compd.* **1996**, *240*, 37–41. [[CrossRef](#)]
24. Wu, P.; Christuk, A.E.; Ibers, J.A. New quaternary chalcogenides  $BaLnMQ_3$  ( $Ln =$  Rare Earth or Sc;  $M = Cu, Ag$ ;  $Q = S, Se$ ). Structure and property variation vs. rare-earth element. *J. Solid State Chem.* **1994**, *110*, 337–344. [[CrossRef](#)]
25. Huang, F.Q.; Mitchell, K.; Ibers, J.A. New layered materials: Syntheses, structures, and optical and magnetic properties of  $CsGdZnSe_3$ ,  $CsZrCuSe_3$ ,  $CsUCuSe_3$ , and  $BaGdCuSe_3$ . *Inorg. Chem.* **2001**, *40*, 5123–5126. [[CrossRef](#)] [[PubMed](#)]
26. Ruseikina, A.V.; Molokeev, M.S.; Chernyshev, V.A.; Aleksandrovsky, A.S.; Krylov, A.S.; Krylova, S.N.; Velikanov, D.A.; Grigoriev, M.V.; Maximov, N.G.; Shestakov, N.P.; et al. Synthesis, structure, and properties of  $EuScCuS_3$  and  $SrScCuS_3$ . *J. Solid State Chem.* **2021**, *296*, 121926. [[CrossRef](#)]
27. Eberle, M.A.; Schleid, T. Expanding the  $SrCuRES_3$  Series with the Rare-Earth Metals Scandium and Yttrium. *Z. Kristallogr.* **2016**, *536*, 71.
28. Ruseikina, A.V.; Solov'ev, L.A. Crystal structures of  $a$ - and  $b$ - $SrCeCuS_3$ . *Russ. J. Inorg. Chem.* **2016**, *61*, 482–487. [[CrossRef](#)]
29. Maier, S.; Prakash, J.; Berthebaud, D.; Perez, O.; Bobev, S.; Gascoin, F. Crystal structures of the four new quaternary copper(I) selenides  $A_{0.5}CuZrSe_3$  and  $ACuYSe_3$  ( $A = Sr, Ba$ ). *J. Solid State Chem.* **2016**, *242*, 14–20. [[CrossRef](#)]
30. Ruseikina, A.V.; Solovyov, L.A.; Grigoriev, M.V.; Andreev, O.V. Crystal structure variations in the series  $SrLnCuS_3$  ( $Ln = La, Pr, Sm, Gd, Er$  and  $Lu$ ). *Acta Crystallogr.* **2019**, *75*, 584–588. [[CrossRef](#)]
31. Sikerina, N.V. Regularities of Phase Equilibria in  $SrS-Ln_2S_3-Cu_2S$  Systems, Preparation and Structure of  $SrLnCuS_3$  Compounds. Ph.D. Thesis, University of Tyumen, Tyumen, Russia, 2005.
32. Ruseikina, A.V.; Demchuk, Z.A. Crystal structure and properties of  $AHoCuS_3$  ( $A = Sr$  or  $Eu$ ). *Russ. J. Inorg. Chem.* **2017**, *62*, 27–32. [[CrossRef](#)]
33. Eberle, M.A. Darstellung und Charakterisierung quaternärer Seltenerdmetall-Verbindungen in Kombination mit Kupfer und Schwefel. Ph.D. Thesis, Stuttgart University, Stuttgart, Germany, 16 December 2016.
34. Ruseikina, A.V.; Grigoriev, M.V.; Solovyov, L.A.; Chernyshev, V.A.; Aleksandrovsky, A.S.; Krylov, A.S.; Krylova, S.N.; Shestakov, N.P.; Velikanov, D.A.; Garmonov, A.A.; et al. A Challenge toward Novel Quaternary Sulfides  $SrLnCuS_3$  ( $Ln = La, Nd, Tm$ ): Unraveling Synthetic Pathways, Structures and Properties. *Int. J. Mol. Sci.* **2022**, *23*, 12438. [[CrossRef](#)] [[PubMed](#)]
35. Strobel, S.; Schleid, T. Three structure types for strontium copper(I) lanthanide(III) selenides  $SrCuMSe_3$  ( $M = La, Gd, Lu$ ). *J. Alloys Compd.* **2006**, *418*, 80–85. [[CrossRef](#)]
36. Strobel, S.; Schleid, T. Quaternary Strontium Copper(I) Lanthanoid(III) Selenides with Cerium and Praseodymium:  $SrCuCeSe_3$  and  $SrCuPrSe_3$ , Unequal Brother and Sister. *Z. Naturforsch.* **2004**, *59b*, 985–991. [[CrossRef](#)]
37. Eberle, M.A.; Strobel, S.; Schleid, T.  $SrCuNdS_3$ : A new Compound with two Different Crystal Structures. *Z. Kristallogr.* **2014**, *534*, 139.
38. Ruseikina, A.V.; Solov'ev, L.A.; Galenko, E.O.; Grigor'ev, M.V. Refined Crystal Structures of  $SrLnCuS_3$  ( $Ln = Er, Yb$ ). *Russ. J. Inorg. Chem.* **2018**, *63*, 1225–1231. [[CrossRef](#)]
39. Ruseikina, A.V.; Andreev, O.V.; Galenko, E.O.; Koltsov, S.I. Trends in thermodynamic parameters of phase transitions of lanthanide sulfides  $SrLnCuS_3$  ( $Ln = La-Lu$ ). *J. Therm. Anal. Calorim.* **2017**, *128*, 993–999. [[CrossRef](#)]
40. Ruseikina, A.V.; Solov'ev, L.A.; Andreev, O.V. Crystal Structures and Properties of  $SrLnCuS_3$  ( $Ln = La, Pr$ ). *Russ. J. Inorg. Chem.* **2014**, *59*, 196–201. [[CrossRef](#)]
41. Grigoriev, M.V.; Solovyov, L.A.; Ruseikina, A.V.; Aleksandrovsky, A.S.; Chernyshev, V.A.; Velikanov, D.A.; Garmonov, A.A.; Molokeev, M.S.; Oreshonkov, A.S.; Shestakov, N.P.; et al. Quaternary Selenides  $EuLnCuSe_3$ : Synthesis, Structures, Properties and In Silico Studies. *Int. J. Mol. Sci.* **2022**, *23*, 1503. [[CrossRef](#)]
42. Sheldrick, G.M. A short history of SHELX. *Acta Crystallogr.* **2008**, *A64*, 112–122.
43. PLATON. *A Multipurpose Crystallographic Tool*; Utrecht University: Utrecht, The Netherlands, 2008.
44. Wakeshima, M.; Furuuchi, F.; Hinatsu, Y. Crystal structures and magnetic properties of novel rare-earth copper sulfides,  $EuRCuS_3$  ( $R = Y, Gd-Lu$ ). *J. Phys. Condens. Matter.* **2004**, *16*, 5503–5518. [[CrossRef](#)]
45. Ruseikina, A.V.; Chernyshev, V.A.; Velikanov, D.A.; Aleksandrovsky, A.S.; Shestakov, N.P.; Molokeev, M.S.; Grigoriev, M.V.; Andreev, O.V.; Garmonov, A.A.; Matigorov, A.V.; et al. Regularities of the property changes in the compounds  $EuLnCuS_3$  ( $Ln = La-Lu$ ). *J. Alloys Compd.* **2021**, *874*, 159968. [[CrossRef](#)]

46. Ruseikina, A.V.; Andreev, O.V. Regularities of change in the structural parameters of  $\text{EuLnCuS}_3$  ( $\text{Ln} = \text{La-Nd, Sm, Gd, Ho}$ ). *Russ. J. Inorg. Chem.* **2017**, *62*, 160–167. [[CrossRef](#)]
47. Shannon, R.D. Revised effective ionic radii and systematic studies of interatomic distances in halides and chalcogenides. *Acta Crystallogr.* **1976**, *A32*, 751–767. [[CrossRef](#)]
48. Baur, W. The geometry of polyhedral distortions. Predictive relationships for the phosphate group. *Acta Crystallogr.* **1974**, *B30*, 1195–1215. [[CrossRef](#)]
49. Mikheykin, A.S.; Chernyshov, D.Y.; Bush, A.A.; Prokhorov, A.S.; Yuzyuk, Y.I.; Dmitriev, V.P. Features of the Jahn-Teller transition in  $\text{Ni}_{1-x}\text{Co}_x\text{Cr}_2\text{O}_4$  solid solutions. *Phys. Solid State* **2014**, *56*, 785–791. [[CrossRef](#)]
50. Yang, L.; Powell, D.R.; Houser, R.P. Structural variation in copper(I) complexes with pyridylmethylamide ligands: Structural analysis with a new four-coordinate geometry index,  $\tau_4$ . *Dalton Trans.* **2007**, *9*, 955–964. [[CrossRef](#)]

**Disclaimer/Publisher's Note:** The statements, opinions and data contained in all publications are solely those of the individual author(s) and contributor(s) and not of MDPI and/or the editor(s). MDPI and/or the editor(s) disclaim responsibility for any injury to people or property resulting from any ideas, methods, instructions or products referred to in the content.